Journal of Electron Spectroscopy and Related Phenomena 256 (2022) 147174

Contents lists available at ScienceDirect

Journal of Electron Spectroscopy and Related Phenomena

journal homepage: www.elsevier.com/locate/elspec

# Auger- and photoelectron coincidences of molecular $O_2$ adsorbed on Ag(111)

F.O.L. Johansson [a,d,*], T. Leitner [b,d], I. Bidermane [b,d], A. Born [b,c,d], A. Föhlisch [b,c,d], S. Svensson [a,d], N. Mårtensson [a,d], A. Lindblad [a,d]

[a] Division of X-ray Photon Science, Department of Physics and Astronomy, Uppsala University, Box 516, 751 20 Uppsala, Sweden
[b] Institute for Methods and Instrumentation in Synchrotron Radiation Research, Helmholtz-Zentrum Berlin für Materialien und Energie GmbH, Albert-Einstein-Strasse 15, 12489 Berlin, Germany
[c] Institut für Physik und Astronomie, Universität Potsdam, Karl-Liebknecht-Strasse 24-25, 14476 Potsdam, Germany
[d] UBjL, Uppsala–Berlin joint Laboratory, Germany

ARTICLE INFO

*Keywords:*
Oxygen/Ag(111)
Auger electron
Photoelectron
Coincidence
APECS
Spectroscopy

ABSTRACT

The oxygen on Ag(111) system has been investigated with Auger electron–photoelectron coincidence spectroscopy (APECS). The coincidence spectra between O *1s* core level photoelectrons and O KLL Auger electrons have been studied together with Ag*3d*/Ag$M_{4,5}$NN coincidences. We also describe the electron–electron coincidence spectrometer setup, CoESCA, consisting of two angle resolved time-of-flight spectrometers at a synchrotron light source. Contributions from molecular oxygen and chemisorbed oxygen are assigned using the coincidence data, conclusions are drawn primarily from the O *1s*/O KLL data. The data acquisition and treatment procedure are also outlined. The chemisorbed oxygen species observed are relevant for the catalytic ethylene oxidation.

## 1. Introduction

### 1.1. Background

The oxygen–Ag system has been the subject of considerable interest from the surface physics community. From the point-of-view of catalysis the certain oxygen sites in the system enable ethylene oxide production ($C_2H_2 + O_2 \rightarrow C_2H_4O$) (or cause a reaction of by-products instead, *eg.* $CO_2 + H_2O$) [1–4] or oxidation of methanol into formaldehyde [5]. From a surface physics perspective the system has attracted interest since oxygen interaction at Ag(111), Ag(110), Ag(100) surfaces exhibit a variation with temperature ranging from physisorption at low temperatures to various stages of dissociative chemisorption, even at room temperature.

Oxygen molecules adsorbed on Ag(111) surfaces do so by physisorption at low temperatures [6]. At liquid helium temperature $O_2$ forms a 2D spin system, which has been imaged directly with scanning tunnelling microscopy [7]. Heating cause dissociation or desorption of adsorbed molecular oxygen between 170–220 K [8]. Atomic oxygen desorbs from the surface at temperatures around 600 K when atoms combine to $O_2$ which may desorb. The intricacies of oxygen interaction with silver including the possibility for diffusion of atomic oxygen into the bulk at temperature slightly above room temperature has been reviewed by van Santen and Kuipers [9] and studied by a battery of methods by Bukhtiyarov and co-workers [8].

The Ag(111)-oxygen system has been investigated in detail using scanning tunnelling microscopy and X-ray photoelectron spectroscopy, which has ultimately given rise to a reinterpretation of the "classical" p(4 × 4) surface oxide of Ag(111) [10,11] – as reviewed by Schnadt and co-workers [12].

### 1.2. Auger electron–photoelectron coincidences

In this article we present results of Auger electron–photoelectron coincidence spectroscopy (APECS) on the Ag 3d/$M_{4,5}$NN and O *1s*/KLL ranges recorded on oxygen adsorbed on Ag(111). For the experiment a new set-up has been used that employ two angle resolved time-of-flight electron analysers (ArTOFs). Before describing the experimental details and results we briefly discuss development of APECS, especially for solids [13–15].

The feasibility of recording Auger- and photoelectrons in coincidence (APECS) was demonstrated already in the late 1970's, The contribution of Cu $2p_{1/2}$ and $2p_{3/2}$ core–hole states to the Cu LMM Auger spectrum were observed [16]. Electron–electron coincidence spectroscopies have been studied using a variety of experimental set-ups [17–22].

By recording the Auger electron and the photoelectron channels in separate instruments within the same time-frame, the data in one

* Corresponding author at: Division of X-ray Photon Science, Department of Physics and Astronomy, Uppsala University, Box 516, 751 20 Uppsala, Sweden.
*E-mail address:* fredrik.johansson@physics.uu.se (F.O.L. Johansson).

https://doi.org/10.1016/j.elspec.2022.147174
Received 3 July 2020; Received in revised form 30 March 2021; Accepted 21 February 2022
Available online 3 March 2022

channel can be filtered using information from the other. This opens up possibilities to study particulars hidden in spectra recorded in only one channel: (a) large surface sensitivity can be achieved by exploring coincidences between the "elastic" photoelectron peak or the "loss"/background at higher biding energies and the Auger spectrum [23–25]; (b) low energy Auger electron spectra can be filtered out of the valence photoelectron background [26], *e.g.* observing the Ag $N_3VV$ Auger spectrum [27]; (c) discriminate between overlapping lines [20,28].

The measured coincidence signal has contributions from two different types of coincidences: true and accidental coincidences. A true coincidence originates from one absorbed photon, creating one electron pair, which leads to one coincidence event in the detectors.

An accidental coincidence occurs, when two or more photons are absorbed and two uncorrelated electrons (thus created by different photons) are detected. The accidental coincidence background is intrinsic to the measurement and there is no possibility to directly discriminate against it.

However, it is possible to infer a dataset with only accidental coincidences by comparing signals in the detectors for pairs of different pulses and count coincidences such as *pulse A, detector 1 with pulse B, detector 2* and, vice versa, comparing *pulse B, detector 1 with pulse A detector 2*. This accidental coincidence dataset can then be subtracted from the total coincidence data-set in order to get the best estimate for true coincidences. For electron–electron coincidences from surfaces, subtraction of the accidental background has previously been demonstrated by Schumann et al. [29].

Coincidence count rates are small (typically around $10^{-6}$/pulse at the used set-up) and the events measured from different pulses are independent from each other. Therefore the coincidences can be described by Poisson statistics. The probability of detecting $k$ events from one pulse for a rate of events per pulse $\lambda$ becomes:

$$P_\lambda(k) = \frac{\lambda^k}{k!} e^{-\lambda} \overset{(\lambda \ll 1)}{\approx} \frac{\lambda^k}{k!} \tag{1}$$

$\lambda$ is linearly proportional to the flux, *i.e.* the number photons per pulse and it is also linked to other experimental parameters, like the total detection volume, detection efficiencies and cross-sections for electron pair creation. A more detailed analysis of the link between electron count rates and experimental parameters may be found in Haak et al. [17] or Jensen et al. [30].

The probabilities for measuring a true coincidence (k=1) or an accidental coincidence (k=2), respectively, read as:

$$\begin{aligned} P_\lambda(1) &\approx \lambda, \\ P_\lambda(2) &\approx \frac{1}{2}\lambda^2. \end{aligned} \tag{2}$$

Accidental coincidences contribution to the signal scales quadratically with respect to the flux — the true coincidences counts scale linearly. Therefore, increasing the flux beyond a certain point will not increase the signal quality anymore, but after that point serve only to increase the accidentals background and hence the amount of data to be stored.

Haak et al. utilised a system with two hemispherical electron energy analysers for APECS [17], something also used in Ref. [31] to study sulphur and oxygen over-layers on nickel; experiments having two cylindrical mirror analysers have been used, which increase the transmission of the system [26]. An angular resolving APECS experiment using seven electron analysers [32] has been used to, for instance, analyse the Ge $2p_{3/2}$ $L_3M_{4,5}M_{4,5}$ system [33].

The system described in this paper consist of two angle resolved time-of-flight spectrometers (ArTOF [34–36]) looking at the same point, as depicted in Fig. 1. Owing to the collection efficiency the ArTOF spectrometer at a pulsed synchrotron X-ray source it has been used to record angle resolved photoelectron spectroscopy (ARPES) data on sensitive samples [37], such as organic single crystals [38]. The full surface band structure can be recorded owing to the 2D and time collection in the data-set, as demonstrated for the topological insulator $Bi_2Se_3$ [39].

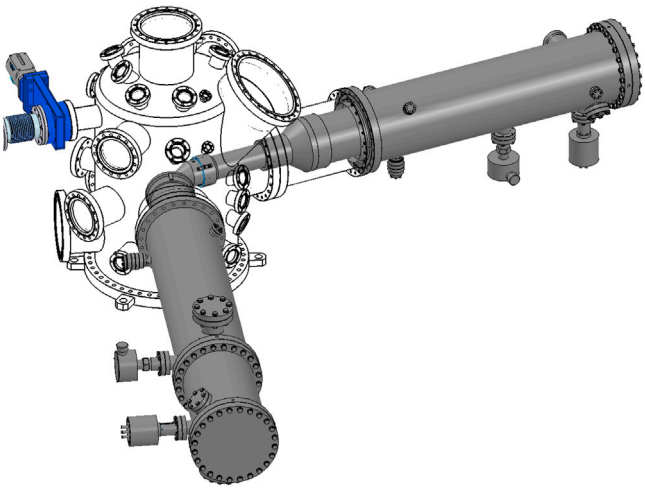

**Fig. 1.** Schematic of the CoESCA measurement setup. The X-rays enter the experiment from the right, and meets the sample in front of the spectrometers. The wide angle ArTOF2-EW is the (grey solid) spectrometer whose backside are outward, the ArTOF−10k protrudes towards right. The manipulator holding the sample is mounted vertically. A spectrometer's flight tube is about 1 m.

A setup that preceded the presently employed system recorded electron–electron coincidences using one ArTOF-spectrometer and one hemispherical electron energy analyser with multi-channel detection. Used, for instance, to study O *1s*/KLL coincidences for gas phase $O_2$ [40,41]. Time-of-flight electron analysers of the ArTOF type increases the transmission, compared to hemispherical analysers, with about two orders of magnitude [37] without sacrificing resolution. This is important when considering Eq. (2) above.

## 2. Experimental

### 2.1. Introduction

Measurements were carried out at the Coincidence Electron Spectroscopy for Chemical Analysis setup (CoESCA) [42] at the UE52-PGM soft X-ray undulator beamline [43] at Helmholtz-Zentrum Berlin, Bessy II. The beamline utilises a plane grating monochromator which was set to 850 eV photon energy for the experiments. From fitting the Ag 3*d* singles spectrum the resolution of the experiment was approximated to 250 meV.

A silver single crystal, Ag(111) (99,999%, MaTecK GmbH), was cleaned by repeated $Ar^+$ sputtering and annealing cycles until a sharp LEED pattern of the surface was obtained. The crystal was cooled to 128 K and subsequently dosed with 500 Langmuirs of $O_2$ (99.999%, Messer AG).

The Ag 3*d*-MNN measurement yielded 161955 coincidence counts from single pulses and 243299 accidental coincidence counts from cross-comparing two consecutive pulses, resulting in 40306 true coincident counts and corresponding to an accidental-to-true ratio of $\nu_a/\nu_t = 6.0$. Measurement time was around 20 h.

The O *1s*-KLL measurement yielded 115769 coincidence counts from single pulses and 135915 accidental coincidence counts from cross-comparing two consecutive pulses, resulting in 47812 true coincident counts and corresponding to an accidental-to-true ratio of $\nu_a/\nu_t = 2.8$. Measurement time was around 47 h.

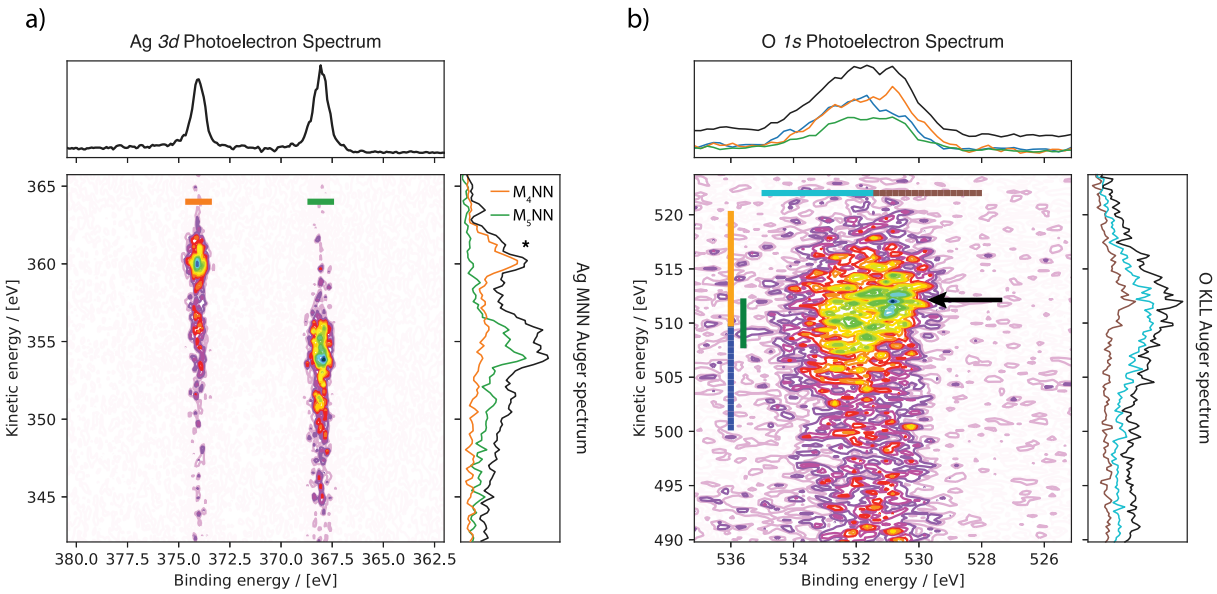


**Fig. 2.** Maps of the (a) Ag *3d*/MNN, and (b) O *1s*/KLL coincidence experiments on $O_2$/Ag(111) presented as contours. The core level photoelectron spectra are presented on top, black lines represent the sum spectra over the entire energy axis. Horizontal and vertical lines in colour on the map indicate ranges of integration for partial sums of Auger and photoelectron spectra respectively. See text for details.

### 2.2. APECS with two ArTOF spectrometers

The monochromatic X-rays were pulsed with a repetition rate of 1.25 MHz. The pulses were obtained through pulse picking through resonant excitation (PPRE) [44] – a running mode of the synchrotron electron storage ring providing pseudo single bunch operation designed to fit with the time-of-flight instrumentation.

At the CoESCA station two ArTOFs are set to measure at the same spot (see Fig. 1). The sample position, the axis along each spectrometer, and the incoming photon beam are in the horizontal plane. The spectrometers are positioned at an angle of ±54.7° with respect to the photon beam. One of the spectrometers (ArTOF−10k) has an angular acceptance of ±14° and one (ArTOF2-EW) with ±24° angular acceptance. The overlap between the volumes analysed is thus large for this setup.

The spectrometers records events at detector coordinates $x, y$ and the time-of-flight of the electron. The data is then converted into two angles and the kinetic energy $E_{kin}$ of the electron. The incoming data is fed to a computer via a Time-to-Digital Converter (TDC) card. The ultimate energy resolution of the spectrometers depends on both the angle and time-resolving capability of the instrument [34]. The computer saves each shot, where at least one ArTOF has seen an electron. Singles[1], and measured, accidental and true coincidences are determined from this list in post processing.

For singles, hits for each spectrometer are counted separately and binned to form a histogram. For measured coincidences — all events, where both spectrometers saw a hit are sorted into a 2D histogram. In order to extract accidental coincidences, the list is parsed for one of the ArTOFs and for each hit, the list for the other ArTOF is checked one shot earlier and one shot later — and if the second ArTOF has seen a hit also, an accidental coincidence is sorted into a 2D-histogram. Since we are then comparing hits from different photon pulses, we are sure that such coincidences are accidental.

The true coincidences are then calculated by subtracting the accidental coincidence map from the measured map [30,42].

The electron analysers of the CoESCA instrument where set to acquire spectra in the kinetic energy regions of Ag MNN Auger electrons (ArTOF−10k), and Ag 3*d* core level photoelectrons (ArTOF2-EW) or, respectively, to the energy regions for O KLL Auger electrons and O *1s* photoelectrons. Energy calibration was performed by recording the Fermi-level of a clean Ag crystal and setting that energy to 0 eV binding energy.

In the kinetic energy ranges used in the this experiment we were operating the ArTOF 2 EW analyser at its design limit. Therefore, the transmission function along the energy window was not constant. We account for this in post-processing by correcting the spectral intensities with a linear transmission function as outlined in Leitner et al. [42]. The ArTOF 10k detector, used for measuring the Auger spectra, was operated well within its specifications, with a constant transmission function.

## 3. Results & discussion

The coincidence datasets are shown as contours in Fig. 2. On top of and, to the right of, each map the intensity integrated over the entire region, and in selected slices are shown. On top these are photoelectron spectra (integrated over kinetic energy axis) and to the right Auger electron spectra (integrated over the binding energy axis). The black trace is the sum of the entire window along one axis, and the coloured horizontal and vertical lines indicate the region of integration that corresponds to a companion integrated spectrum (presented in the same colour) in the 1D plots.

### 3.1. Silver APECS

The Ag APECS results are presented in Fig. 2a, the $M_4NN$ and $M_5NN$ Auger features can be discerned already in the map owing to the well separated spin–orbit components of the Ag 3*d* photoelectron spectrum (6.0 eV spin–orbit energy split in metallic Ag [45]).

The ratio between the areas of the Ag 3*d* components is not what is expected from a $5/2 - 3/2$ multiplet. A least squares fit to the spectrum finds a spin–orbit split of 5.99 eV (found for metallic silver and oxide compounds [45,46]) and result in a ratio of 1.31 between the areas of the components. The deviation from the expected statistical ratio of 1.5 can be explained by the fact that we have parts of the Auger signal outside of our detection region, therefore coincidences from those will not be included as such owing to the finite detection window.

[1] *i.e.* a spectrum in one channel, such as a core level spectrum which is unfiltered with regards to the other channel.

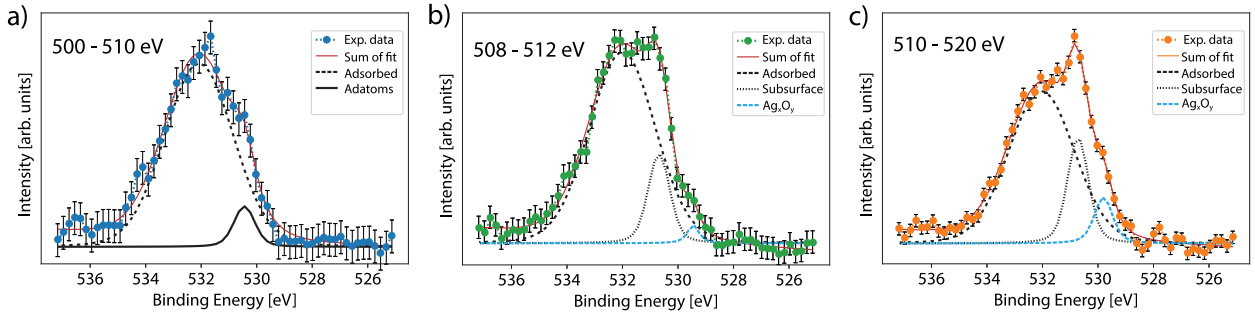


**Fig. 3.** O *1s* photoelectron spectra corresponding to sub-sets of the coincidence map created by integrating parts of the kinetic energy axis (panel a: 500–510 eV kinetic energy, b: 508–512 eV and c: 510–520 eV). The least squares fit result are included as a solid (red) line. In panel (a) two components account for the spectrum and in (b) and (c) three components were used. The ratio between the main component and the other component(s) are 14 in panel (a) and 5 and 3 in panels (b) and (c) respectively. See text for detailed interpretation.

The Ag 3*d* energy level has a large cross section, well separated components, and with a relatively narrow natural line width [46]. This allows for filtering out details in the Auger channel belonging to either spin–orbit component. These are the Auger spectra in orange and blue respectively. For instance, we can see that the $M_4NN$ channel (orange) has a broadening towards lower kinetic energies, and thus overlap with the $M_5NN$ (green) channel.

The APECS spectrum of Ag 3*d*/MNN has been thoroughly studied [20,21,47,48], there is also a theoretical description [49]. Comparing our filtered MNN spectra with those of [21] the main spectral features are similar. However, the shoulder at higher kinetic energy in the $M_4NN$ (marked with *) is more pronounced in our data due to higher resolution in the measurement. The similarity with the clean silver data from Arena et al. [21] suggest that the interaction between the $O_2$ and the Ag(111) substrate is weak — as has been observed previously [50]. If the silver surface would be oxidised the spectral features of the Auger lines would be broadened and the shoulder would be less pronounced [45,51].

The kinetic energy position of the Ag MNN Auger spectrum agrees with Ferraria et al. [45], but differs from Arena et al. [21]. We have calibrated the kinetic energy scale using the Fermi-level of Ag(111) and the discrepancy may arise from the choice of work-function, here it does not affect the conclusions.

### 3.2. Oxygen APECS

The main intensity of the oxygen APECS map in Fig. 2b can be seen between 530–532 eV binding energy and 510–515 eV kinetic energy. The highest intensity is at 512 eV kinetic and 531 eV binding energy (marked with the arrow), this point is separated from a broader feature at higher binding energy (in the range of the cyan line). These two regions have been integrated over the partial binding energy ranges indicated, and yields the partial Auger spectra seen to the right. The two regions are chosen similarly to that of the gas-phase $O_2$ APECS by Arion et al. [40], in that instance it is the O *1s* gerade and ungerade components. In our data this corresponds to regions previously identified as two components in the O *1s* spectrum of adsorbed oxygen on silver by Schnadt et al. [12]. The kinetic energy axis is cut so that the majority of the intensity from the brown Auger spectrum is in one slice and the rest in another, these are the orange and blue lines and integrated photoelectron spectra respectively. A small overlap region included for discussion, in green, is also integrated as an intermediate between the two regions. These XPS spectra reveals more structure and they were fitted using a least squares method. The results of fits using three symmetric Voigt line-shapes and a linear background function are presented in Fig. 3.

As mentioned above, free molecular oxygen has been investigated with electron–electron coincidences using ArTOF and a hemispherical electron energy analyser [40,41]. Qualitatively the photoelectron–Auger electron coincidences of that study are similar to our oxygen data in Fig. 2b, albeit shifted and broadened. In Fig. 2 the O KLL Auger spectra that corresponds to partial summations towards higher and lower binding energies are different. The region at 510 eV kinetic energy and below in (the brown spectrum) has considerably less intensity than the cyan equivalent (integrated between 528 and 531 eV binding energy). The other Auger partial spectrum (cyan) carry intensity in that region and has the same intensity distribution as the gas phase APECS spectrum [40]. The Auger spectrum from the brown region is primarily from a core-ionisation on the subsurface oxygen species which have a distinctly different relaxation pathway compared to the Auger spectrum dominated by the adsorbed molecular oxygen (cyan spectrum). The assignment of the oxygen species is discussed below.

**Table 1**
Oxygen moieties and their respective O *1s* binding energies from the fits in Fig. 3. See text for details.

| O *1s* B.E. [eV] | Oxygen moiety |
|---|---|
| 532.0±0.1 | Adsorbed molecular $O_2$ [54] |
| 530.7±0.04 | Subsurface atomic oxygen in interstitial sites [55] |
| 530.4±0.15 | Oxygen ad-atoms [50] |
| 529.8±0.1<br>529.5±0.1 | Surface oxide [56,57] |

Partial oxygen core level spectra have been created through summations over 510–520 eV and 500–510 eV kinetic energy. The former has a feature between 531 and 529 eV as seen in Fig. 2 that seems absent in the other spectrum. Least squares fits to those O *1s* spectra are presented in Fig. 3. The fits were carried out using the lmfit package [52] in Python. The spectra were fitted with three Voigt functions using a life-time broadening of 140 meV (from O *1s* photoelectron spectrum of $O_2$ in the gas-phase [53]). The error bars are the standard deviation for the different partial spectra are calculated from the background from 528 eV binding energy and below.

To account for the intensity distribution in the spectra it turns out that a component in the 531 and 529 eV region persist in all spectra — otherwise dominated by a large component at 532 eV (having 4 eV FWHM). A third component account for the low binding energy shoulder in Fig. 3b and c. The ratio between the main component and the other component(s) are 13 and 3 respectively in the partial spectra from non-overlapping regions. The second and third components have FWHMs around 1 eV.

The energy positions of the components are given in Table 1. The main component in all spectra is at $532.0 \pm 0.1$ eV binding energy. This is the binding energy that physisorbed molecular oxygen is expected to have [54]. Considering that we does our Ag crystal at cryogenic temperatures it is not unexpected that this component dominate the oxygen core level spectrum.

The low binding energy shoulder in Fig. 3a is at a binding energy of $530.4 \pm 0.15$ eV whereas the component giving the second most intense peak in panels b and c are at $530.7 \pm 0.04$ eV. The latter is assigned to oxygen atoms beneath or inside the Ag surface in interstitial sites [55]. The $530.4 \pm 0.15$ eV component has been assigned to oxygen ad-atoms from dissociated oxygen molecules [50].

Rajumon et al. [54] have investigated the O *1s* core level photoelectron spectrum of $O_2$ adsorbed on low index surfaces of Ag single crystals varying the temperature between 100 K and 300 K. They observe two peaks for 500 L of $O_2$ at 530 and 532 eV up to room temperature. The lower binding energy feature remain upon heating to 300 K whereas the surface molecular oxygen diminish [54].

In the silver–oxygen system the oxygen photoelectron spectrum exhibit negative shifts with increasing association with the silver substrate. The progression of chemical shifts in Table 1 follow this trend. The surface oxide that we assign between 529.8 and 529.5 eV are slightly higher in binding energy than that reported by Kaspar et al. [57]. The stoichiometric oxides AgO and $Ag_2O$ have binding energies at 528.4 and 529.2 eV respectively [58]. With chemisorbed atomic oxygen at 530.4 eV and subsurface oxygen at 530.7 eV we tentatively assign the lowest binding energy shoulder we observe to non-stoichiometric $Ag_xO_y$ formed on the surface. It should be noted that the probability of formation of an oxide is low at these experimental temperatures. However, we do observe components in the O *1s* partial sum spectrum that have energies close to that would be expected of an oxide. Further investigation into the origin of these components is required to definitely assign these features.

Looking at the full sum O *1s* core-level spectrum in Fig. 2b it is not obvious that this structure is built up from the four components that we have identified through the partial sums using the Auger spectra as filter (as further discussed in the supplementary information). We have also shown that an overlapping region can be extracted to facilitate the least squares interpretation of the data.

## 4. Summary & conclusion

APECS, and considerations for electron–electron coincidence instrumentation has briefly been highlighted. The CoESCA experiment and the data acquisition and treatment procedure have been outlined (detailed in Leitner et al. [42]).

We have presented the first APECS results using the CoESCA station at Helmholtz-Zentrum Berlin on $O_2$ molecular absorption on a cooled Ag(111) single crystal. Both contributions from molecular oxygen and what is attributed to chemisorbed oxygen are assigned. We have demonstrated the capability of using the partial core level photoelectron spectra to assign various chemical species in a complex system such as Ag-O. For applications this is attractive since the same species may be catalytically active and inactive depending on the chemical environment, e.g. oxygen is relevant for catalytic ethylene oxidation but some adsorption sites are inactive in that reaction. For high pressure oxygen dosing on Ag(111) at room temperature, the oxygen species observed at around 530 eV are attributed to species catalytically active that reside on the surface [8,59].

In conclusion, APECS spectroscopy has developed from an origin using two hemispherical analysers in the end of the 1970s to the utilisation of parallel multidimensional acquisition in time-of-flight electron energy analysers. This development is in principle made possible with the advent of enough computer power to handle and analyse the data-flow within a reasonable time-frame.

The increase in transmission can be used to gain higher discrimination since the basic rules of the game stipulate that counting rates need to be kept low. Since the details resolvable become more fine grained, using this piece of instrumentation for APECS good things may indeed come to those who wait.

## Acknowledgements

We thank HZB for the allocation of synchrotron radiation beamtime. This project has received funding from the European Union's Horizon 2020 research and innovation programme under grant agreement No 730872. A.L. acknowledges the support from the Swedish Research Council (grant no. 2014-6463 and 2018-05336) and Marie Skłodowska Curie Actions (Co-fund, Project INCA 600398). F.J. acknowledges financial support from the K G Westman foundation.

## Appendix A. Supplementary data

Supplementary material related to this article can be found online at https://doi.org/10.1016/j.elspec.2022.147174.

## References

[1] Xenopiion E. Verykios, Fred P. Stein, Robert W. Coughlin, Oxidation of ethylene over silver: adsorption, kinetics, catalyst, Catal. Rev.—Sci. Eng. 22 (2) (1980) 197–234.
[2] Robert B. Grant, Richard M. Lambert, A single crystal study of the silver-catalysed selective oxidation and total oxidation of ethylene, J. Catal. 92 (2) (1985) 364–375.
[3] V.I. Bukhtiyarov, A.I. Boronin, V.I. Savchenko, Stages in the modification of a silver surface for catalysis of the partial oxidation of ethylene: I. Action of oxygen, J. Catal. 150 (2) (1994) 262–267.
[4] Tiancheng Pu, Huijie Tian, Michael E Ford, Srinivas Rangarajan, Israel E Wachs, Overview of selective oxidation of ethylene to ethylene oxide by Ag catalysts, ACS Catal. 9 (12) (2019) 10727–10750.
[5] M. Avramov-Ivić, S. Štrbac, V. Mitrović, The electrocatalytic properties of the oxides of noble metals in the electrooxidation of methanol and formic acid, Electrochim. Acta 46 (20-21) (2001) 3175–3180.
[6] Yoshinori Kazama, Masuaki Matsumoto, Toshiki Sugimoto, Tatsuo Okano, Katsuyuki Fukutani, Low-temperature surface phase and phase transition of physisorbed oxygen on the Ag (111) surface, Phy. Rev. B 84 (6) (2011) 064128.
[7] Shunji Yamamoto, Yasuo Yoshida, Hiroshi Imada, Yousoo Kim, Yukio Hasegawa, Direct visualization of surface phase of oxygen molecules physisorbed on Ag(111) surface: A two-dimensional quantum spin system, Phys. Rev. B 93 (2016) 081408.
[8] V.I. Bukhtiyarov, V.V. Kaichev, E.A. Podgornov, I.P. Prosvirin, XPS, UPS, TPD and TPR studies of oxygen species active in silver-catalysed ethylene epoxidation, Catal. Lett. 57 (4) (1999) 233–239.
[9] R.A. Van Santen, HPCE Kuipers, The mechanism of ethylene epoxidation, in: Advances in Catalysis, Vol. 35, Elsevier, 1987, pp. 265–321.
[10] Angelos Michaelides, Karsten Reuter, Matthias Scheffler, When seeing is not believing: oxygen on Ag (111), A simple adsorption system?, J. Vac. Sci. Technol. A 23 (6) (2005) 1487–1497.
[11] Joachim Schnadt, Angelos Michaelides, Jan Knudsen, Ronnie Thorbjørn Vang, Karsten Reuter, Erik Lægsgaard, Matthias Scheffler, Flemming Besenbacher, Revisiting the structure of the p (4× 4) surface oxide on Ag (111), Phys. Rev. Lett. 96 (14) (2006) 146101.
[12] Joachim Schnadt, Jan Knudsen, Xiao Liang Hu, Angelos Michaelides, Ronnie T Vang, Karsten Reuter, Zheshen Li, Erik Lægsgaard, Matthias Scheffler, Flemming Besenbacher, Experimental and theoretical study of oxygen adsorption structures on Ag (111), Phy. Rev. B 80 (7) (2009) 075424.
[13] S. M. Thurgate, Auger photoelectron coincidence spectroscopy, J. Electron Spectrosc. Relat. Phenom. 100 (1-3) (1999) 161–165.
[14] G Stefani, R Gotter, A Ruocco, F Offi, F Da Pieve, S Iacobucci, A Morgante, A Verdini, A Liscio, H Yao, et al., Photoelectron–auger electron coincidence study for condensed matter, J. Electron Spectrosc. Relat. Phenom. 141 (2-3) (2004) 149–159.
[15] R.A. Bartynski, E. Jensen, S.L. Hulbert, C.-C. Kao, Auger photoelectron coincidence spectroscopy using synchrontron radiation, Prog. Surf. Sci. 53 (2-4) (1996) 155–162.
[16] H.W. Haak, G.A. Sawatzky, T.D. Thomas, Auger-photoelectron coincidence measurements in copper, Phys. Rev. Lett. 41 (26) (1978) 1825.
[17] HW Haak, GA Sawatzky, L Ungier, JK Gimzewski, TD Thomas, Core-level electron–electron coincidence spectroscopy, Rev. Sci. Instrum. 55 (5) (1984) 696–711.
[18] Xinjuan Liu, Xi Zhang, Maolin Bo, Lei Li, Hongwei Tian, Yanguang Nie, Yi Sun, Shiqing Xu, Yan Wang, Weitao Zheng, Chang Q Sun, Coordination-resolved electron spectrometrics, Chem. Rev. 115 (14) (2015) 6746–6810.
[19] Tiberiu Arion, Uwe Hergenhahn, Coincidence spectroscopy: past, present and perspectives, J. Electron Spectrosc. Relat. Phenom. 200 (2015) 222–231.
[20] D.A. Arena, R.A. Bartynski, S.L. Hulbert, A method for determining intrinsic shapes of overlapping spectral lines in auger-photoelectron coincidence spectroscopy, Rev. Sci. Instrum. 71 (4) (2000) 1781–1787.

[21] DA Arena, RA Bartynski, RA Nayak, AH Weiss, SL Hulbert, Line shape of the Ag M4,5VV auger spectra measured by auger-photoelectron coincidence spectroscopy, Phy. Rev. B 63 (15) (2001) 155102.

[22] Grant Van Riessen, Zheng Wei, Rajendra S Dhaka, Carsten Winkler, Frank O Schumann, Jürgen Kirschner, Direct and core-resonant double photoemission from Cu (001), J. Phys.: Condens. Matter 22 (9) (2010) 092201.

[23] Wolfgang S.M. Werner, Herbert Störi, Hannspeter Winter, Quantitative model for the surface sensitivity in auger-photoelectron coincidence spectroscopy (APECS), Surf. Sci. 518 (1-2) (2002) L569–L576.

[24] A Liscio, R Gotter, A Ruocco, S Iacobucci, AG Danese, RA Bartynski, G Stefani, Experimental evidence for extreme surface sensitivity in auger-photoelectron coincidence spectroscopy (APECS) from solids, J. Electron Spectrosc. Relat. Phenom. 137 (2004) 505–509.

[25] Wolfgang SM Werner, Werner Smekal, Herbert Störi, Hannspeter Winter, Giovanni Stefani, Alessandro Ruocco, Francesco Offi, Roberto Gotter, Alberto Morgante, Fernando Tommasini, Emission-depth-selective auger photoelectron coincidence spectroscopy, Phys. Rev. Lett. 94 (3) (2005) 038302.

[26] S. Satyal, P.V. Joglekar, K. Shastry, S. Kalaskar, Q. Dong, S.L. Hulbert, R.A. Bartynski, A.H. Weiss, Measurement of the background in auger-photoemission coincidence spectra (APECS) associated with inelastic or multi-electron valence band photoemission processes, J. Electron Spectrosc. Relat. Phenom. 195 (2014) 66 – 70.

[27] PV Joglekar, RW Gladen, VA Chirayath, AJ Fairchild, S Kalaskar, K Shastry, Q Dong, SL Hulbert, RA Bartynski, WSM Werner, et al., Measurement of the full electron spectrum associated with the Ag N3VV auger transitions: evidence for the contribution of multi-electron auger processes, J. Electron Spectrosc. Relat. Phenom. 235 (2019) 16–22.

[28] R Gotter, F Offi, F Da Pieve, A Ruocco, G Stefani, S Ugenti, MI Trioni, RA Bartynski, Electronic and magnetic properties of thin films probed by auger photoelectron coincidence spectroscopy (APECS), J. Electron Spectrosc. Relat. Phenom. 161 (1-3) (2007) 128–133.

[29] F. O. Schumann, R. S. Dhaka, G. A. Van Riessen, Z. Wei, J. Kirschner, Surface state and resonance effects in electron-pair emission from Cu(111), Phys. Rev. B 84 (2011) 125106.

[30] E. Jensen, R. A. Bartynski, S. L. Hulbert, E. D. Johnson, Auger photoelectron coincidence spectroscopy using synchrotron radiation, Rev. Sci. Instrum. 63 (1992) 3013.

[31] G. Di Filippo, F.O. Schumann, S. Patil, Z. Wei, G. Stefani, G. Fratesi, M.I. Trioni, J. Kirschner, Electron coincidence studies of sulfur-overlayers on Cu(001) and Ni(001) surfaces, J. Electron Spectrosc. Relat. Phenom. 211 (2016) 32 – 40.

[32] R Gotter, A Ruocco, A Morgante, D Cvetko, L Floreano, F Tommasini, G Stefani, The ALOISA end station at elettra: A novel multicoincidence spectrometer for angle resolved APECS, Nucl. Instrum. Methods Phys. Res. A 467 (2001) 1468–1472.

[33] R Gotter, A Ruocco, MT Butterfield, S Iacobucci, G Stefani, RA Bartynski, Angle-resolved auger-photoelectron coincidence spectroscopy (AR-APECS) of the Ge (100) surface, Phy. Rev. B 67 (3) (2003) 033303.

[34] Gunnar Öhrwall, P Karlsson, M Wirde, M Lundqvist, Pontus Andersson, Denis Ceolin, B Wannberg, T Kachel, H Dürr, W Eberhardt, et al., A new energy and angle resolving electron spectrometer–first results, J. Electron Spectrosc. Relat. Phenom. 183 (1-3) (2011) 125–131.

[35] R Ovsyannikov, P Karlsson, M Lundqvist, C Lupulescu, W Eberhardt, A Föhlisch, S Svensson, N Mårtensson, Principles and operation of a new type of electron spectrometer–ArTOF, J. Electron Spectrosc. Relat. Phenom. 191 (2013) 92–103.

[36] T Abukawa, S Yamamoto, R Yukawa, S Kanzaki, K Mukojima, I Matsuda, Time-resolved soft x-ray core-level photoemission spectroscopy at 880° C using the pulsed laser and synchrotron radiation and the pulse heating current, Surf. Sci. 656 (2017) 43–47.

[37] Erika Giangrisostomi, Ruslan Ovsyannikov, Florian Sorgenfrei, Teng Zhang, Andreas Lindblad, Yasmine Sassa, Ute B Cappel, Torsten Leitner, Rolf Mitzner, Svante Svensson, et al., Low dose photoelectron spectroscopy at BESSY II: electronic structure of matter in its native state, J. Electron Spectrosc. Relat. Phenom. 224 (2018) 68–78.

[38] A Vollmer, R Ovsyannikov, M Gorgoi, S Krause, M Oehzelt, A Lindblad, N Mårtensson, S Svensson, P Karlsson, M Lundvuist, et al., Two dimensional band structure mapping of organic single crystals using the new generation electron energy analyzer ARTOF, J. Electron Spectrosc. Relat. Phenom. 185 (3-4) (2012) 55–60.

[39] PDC King, RC Hatch, M Bianchi, R Ovsyannikov, C Lupulescu, G Landolt, B Slomski, JH Dil, D Guan, JL Mi, et al., Large tunable rashba spin splitting of a two-dimensional electron gas in Bi2Se3, Phys. Rev. Lett. 107 (9) (2011) 096802.

[40] Tiberiu Arion, Ralph Püttner, Cosmin Lupulescu, Ruslan Ovsyannikov, Marko Förstel, Gunnar Öhrwall, Andreas Lindblad, Kiyoshi Ueda, Svante Svensson, Alex M Bradshaw, et al., New insight into the auger decay process in O2: the coincidence perspective, J. Electron Spectrosc. Relat. Phenom. 185 (8-9) (2012) 234–243.

[41] C Lupulescu, T Arion, U Hergenhahn, R Ovsyannikov, M Förstel, G Gavrila, W Eberhardt, iDEEAA: A novel, versatile apparatus for electron spectroscopy, J. Electron Spectrosc. Relat. Phenom. 191 (2013) 104–111.

[42] T. Leitner, A. Born, I. Bidermane, R. Ovsyannikov, F. O. L. Johansson, Y. Sassa, A. Föhlisch, A. Lindblad, F. O. Schumann, S. Svensson, N. Mårtensson, The CoESCA station at BESSY: auger electron-photoelectron coincidences from surfaces demonstrated for Ag MNN, J. Electron Spectrosc. Relat. Phenom. 250 (2021) 147075.

[43] Ruslan Ovsyannikov, Tobias Lau, The variable polarization undulator beamline UE52 PGM nanocluster trap at BESSY II, J. Large-Scale Res. Facil. JLSRF 3 (2017) 105.

[44] K Holldack, R Ovsyannikov, P Kuske, R Müller, A Schälicke, M Scheer, M Gorgoi, D Kühn, T Leitner, S Svensson, et al., Single bunch x-ray pulses on demand from a multi-bunch synchrotron radiation source, Nat. Commun. 5 (1) (2014) 1–7.

[45] Ana Maria Ferraria, Ana Patrícia Carapeto, Ana Maria Botelho do Rego, X-ray photoelectron spectroscopy: silver salts revisited, Vacuum 86 (12) (2012) 1988–1991.

[46] Nils Mårtensson, Ralf Nyholm, Electron spectroscopic determinations of $M$ and $N$ core-hole lifetimes for the elements Nb—Te ($Z = 41 - 52$), Phys. Rev. B 24 (1981) 7121–7134.

[47] S.M. Thurgate, C.P. Lund, Comparison of the auger photoelectron coincidence spectroscopy (APECS) spectra of Ag and InP with Cu and GaAs, Surf. Interface Anal. 25 (1) (1997) 10–16.

[48] Z.T. Jiang, M. Ohno, S.M. Thurgate, G. Van Riessen, The M5 photoelectron line of Ag metal measured in coincidence with the M5–N45N45 auger-electron spectral line, J. Electron Spectrosc. Relat. Phenom. 143 (1) (2005) 33–37.

[49] Masahide Ohno, Analysis of the auger-photoelectron coincidence spectroscopy (APECS) spectra of metallic Pd, Ag, and Sn, J. Electron Spectrosc. Relat. Phenom. 148 (1) (2005) 47–57.

[50] C. Rehren, M. Muhler, X. Bao, R. Schlögl, G. Ertl, The interaction of silver with oxygen, Z. Phys. Chem. 174 (1) (1991) 11–52.

[51] G Schön, J Tummavuori, B Lindström, CR Enzell, CG Swahn, ESCA studies of Ag, Ag2O and AgO, Acta Chem. Scand 27 (7) (1973) 2623.

[52] Matthew Newville, Till Stensitzki, Daniel B. Allen, Antonino Ingargiola, LMFIT: Non-Linear Least-Square Minimization and Curve-Fitting for Python, Zenodo, 2014.

[53] SL Sorensen, KJ Børve, R Feifel, A De Fanis, Kiyoshi Ueda, The o 1s photoelectron spectrum of molecular oxygen revisited, J. Phys. B: At. Mol. Opt. Phys. 41 (9) (2008) 095101.

[54] M.K. Rajumon, K. Prabhakaran, CNR Rao, Adsorption of oxygen on (100),(110) and (111) surfaces of Ag, Cu and Ni: An electron spectroscopic study, Surf. Sci. 233 (1-2) (1990) L237–L242.

[55] M Rocca, L Savio, L Vattuone, U Burghaus, V Palomba, N Novelli, F Buatier de Mongeot, U Valbusa, R Gunnella, G Comelli, et al., Phase transition of dissociatively adsorbed oxygen on Ag (001), Phy. Rev. B 61 (1) (2000) 213.

[56] Dirk Lützenkirchen-Hecht, Hans-Henning Strehblow, Anodic silver (II) oxides investigated by combined electrochemistry, ex situ XPS and in situ x-ray absorption spectroscopy, Surf. Interface Anal. 41 (10) (2009) 820–829.

[57] Tiffany C Kaspar, Tim Droubay, Scott A Chambers, Paul S Bagus, Spectroscopic evidence for Ag (III) in highly oxidized silver films by x-ray photoelectron spectroscopy, J. Phys. Chem. C 114 (49) (2010) 21562–21571.

[58] Gar B. Hoflund, Zoltan F. Hazos, Ghaleb N. Salaita, Surface characterization study of Ag, AgO, and Ag2O using x-ray photoelectron spectroscopy and electron energy-loss spectroscopy, Phy. Rev. B 62 (16) (2000) 11126.

[59] V.I. Bukhtiyarov, V.V. Kaichev, I.P. Prosvirin, Oxygen adsorption on Ag (111): x-ray photoelectron spectroscopy (XPS), angular dependent x-ray photoelectron spectroscopy (ADXPS) and temperature-programmed desorption (TPD) studies, J. Chem. Phys. 111 (5) (1999) 2169–2175.